Chapter 2

Metal Adsorption by Coal Fly Ash: The Role of Nano-sized Materials

Anita Etale, Nikita T. Tavengwa and Vusumzi E. Pakade

Additional information is available at the end of the chapter

http://dx.doi.org/10.5772/intechopen.69426

Abstract

Nano-sized particles (1–100 nm) comprise a considerable fraction of coal fly ash (CFA). They are unique due to their large surface area and higher reactivity compared to larger CFA particles. As they are formed by nucleation of volatilised elements or through chemical reactions, nano-scale CFA particles have been shown to take up greater quantities of elemental ions and bind them more strongly than larger particles, diminishing the fraction of desorbed ions. Despite this and the large volume of literature on acid mine drainage (AMD) treatment using CFA, little is described about the specific role of nanoparticles in this process. This chapter therefore sets out to highlight this, beginning by delineating nanoparticle characteristics that make them good adsorbents followed by details of their formation and action in metal adsorption.

Keywords: nanoparticles, acid mine drainage, remediation, mining, water pollution

1. Introduction

Coal accounts for up to 29% of energy production worldwide, generating millions of tons of incombustible residue known as coal fly ash (CFA) in the process [1]. The colour of CFA varies from tan to grey to black depending on the amount of unburnt carbon. It consists of fine spherical particles that may be either hollow or solid and have surface areas as high as 1000 $m^2 kg^{-1}$ [2].

The chemical properties of CFA are primarily influenced by the type of coal burnt, that is, bituminous, sub-bituminous, anthracite or lignite. Anthracite has the highest carbon content, hence also has the highest calorific value of all four types. It however, costs two to three times

more than regular coal and is therefore not typically used in commercial boilers. Bituminous coal contains mostly silica, alumina, iron oxide and calcium while lignite and sub-bituminous coal contain less silica and iron oxides but higher calcium and magnesium oxide concentrations (**Table 1**). CFA is also designated based on the concentrations of these four major minerals. Ash with more than 70 wt% silica, alumina and iron oxides and low in lime (1–12%) is designated class F while ash with 50–70 wt% silica, alumina and iron oxides and high lime content (30–40%) is class C [2]. The former is usually produced from combustion of bituminous and anthracite coal, and the latter from lignite and sub-bituminous coals.

Although the greater share of CFA generated after coal combustion is deposited in waste heaps, it is also widely used in road construction, as a raw material in cement manufacture, for the sequestration of toxic gases including SO_2, NO_2 and Hg and, more recently, as a source of catalysts and metals [3, 4].

The formation of mine drainage laden with toxic concentrations of metals and other ions is a common legacy of base metal and coal mining [5, 6]. Acid mine drainage (AMD) is formed via a cascade of reactions when ferrous sulphide phases, for example, pyrite are exposed to oxygenated water, leading to the formation of ferric ion. Ferric ion then subsequently acts as an additional oxidising agent for pyrite, making the reaction self-perpetuating as long as the pH remains below 3.5 although other factors, including temperature and microorganisms, also play an important role [7]. AMD poses significant environmental and ecological challenges to receiving water bodies as well as to human populations that depend on these water resources for consumption [8]. There have therefore been numerous attempts at investigating the use of various materials including CFA which is otherwise a waste product, for the treatment of AMD. Two main characteristics stand out in favour of CFA: (i) its alkaline nature that counters AMD acidity and (ii) its capacity for adsorption/co-precipitation of elemental ions [9, 10]. The synthesis of other adsorbents from CFA, for example, zeolites [11–16], modified mesoporous silica [17] and a number of other composite materials [18–20] have also been widely studied.

Metal removal by CFA and its derivatives varied, following different mechanisms including ion exchange, precipitation as well as chemical and physical adsorption as the following

Components	Bituminous (%)	Sub-bituminous (%)	Lignite (%)
Silica	20–60	40–60	15–45
Alumina	5–35	20–30	10–25
Ferric oxide	10–40	4–10	4–15
Calcium oxide	1–12	5–30	15–40
Magnesium oxide	0–5	1–6	3–10
Sulphite	0–4	0–2	0–10
Sodium oxide	0–4	0–2	0–6
Potassium oxide	0–3	0–4	0–4

Table 1. Chemical composition of fly ash from the combustion of bituminous, sub-bituminous and lignite coal [2].

selected examples illustrate. Belviso et al. [12] investigated the removal of Mn^{2+} by raw CFA from Brindisi, Italy, and a zeolite synthesised from the same fly ash. They found that adsorption was rapid, attaining equilibrium in 5 minutes and that samples filtered with untreated CFA which contained higher Ca^{2+} and Mg^{2+} concentrations, for example, up to 340 mg L^{-1} versus 22 mg L^{-1} of Ca in CFA and zeolite-treated samples, respectively. In addition, although CFA resulted in slightly greater removal in both batch and column tests, >97% of Mn^{2+} was removed from solution by the end of exposure times. With pH_{PZC} of 12.2 and 12, adsorption of Mn^{2+} to either adsorbents was unlikely as all were positively charged. Since Mn^{2+} precipitates above pH 9 as $Mn(OH)_2$, the high solution pH induced by adsorbents likely resulted in its precipitation. These high efficiencies were therefore the result of Mn^{2+} precipitation induced by the high pH of the adsorbents. Indeed, as noted by Cho et al. [9], fly ash is strongly alkaline with pH ranging from 10 to 13 when added to water. In contrast to the preceding study, these authors found that their CFA, sourced from Boryug, Korea, had a pH_{PZC} of 2.8. It was therefore primed for adsorption of positively charged metal ions over a wide pH range and indeed, removed >95% of Zn^{2+}, Pb^{2+}, Cd^{3+} and Cu^{2+} by pH 8. Further, although removal of Zn was reduced in the presence of Cu^{2+} and Pb^{2+}, that of Cd^{3+} was improved in the presence of Pb^{2+}, and removal of Pb^{2+} itself was unaffected by any of the other metals. In general, adsorption by this CFA was in the order of $Pb^{2+} > Cu^{2+} > Cd^{3+} > Zn^{2+}$. Adsorption equilibrium was attained in 2 hours for Zn and in 3 hours for the rest of the metals, and isotherm data for all four were well fitted by the Freundlich isotherm.

Spherical porous pellets made from Class C CFA from power plant in Greece were used by Papandreou et al. [21] and applied in the removal of Pb^{2+}, Zn^{2+} and Cr^{3+}. The pellets had a Brunauer-Emmett-Teller surface area of 23.41 m^2 g^{-1} and approximately 52% of pore volumes occupied by 3.5–4.5 nm pores. Adsorption was investigated at pH 1–10 and found to be optimal at pH 7, for Pb^{2+} and Cr^{2+} and pH 8 for Zn^{2+}. Electrostatic attraction between the ions and the charged adsorbent surface was determined to be the adsorption mechanism. Adsorption isotherms were best fitted by the Langmuir isotherm and maximum adsorption capacities of the pellets calculated to be 0.22, 0.27and 0.44 mmol g^{-1} for Pb^{2+}, Zn^{2+} and Cr^{3+}, respectively. Zinc adsorption was strongly inhibited in the presence of Pb, a finding similar to that of Cho et al. [9] above, and which implies that these ions sorb to similar sites on both types of CFA. In contrast, Cr^{3+} did not inhibit sorption of either Pb^{2+} or Zn^{2+}.

The relationship between adsorption and temperature is often used as an indicator of whether the process involves chemical or physical bond formation. An inverse relationship, that is, where adsorption decreases with increasing temperature denotes physisorption while a direct relationship, that is, adsorption increasing with increasing temperature denotes chemisorption. Adsorption to the pellets in the study by Papandreou above was found to substantially increase with temperature from 25 to 60°C implying that sorption of Pb^{2+}, Zn^{2+} and Cr^{3+} was via chemical bond formation.

The use of CFA for the adsorption of metal ions from acid mine drainage was investigated by Rios et al. [22]. A class F CFA from the Rugeley power station in the West Midlands of England was applied to the strongly acidic (pH < 2) AMD from the Parys mountain in Anglesley, North Wales. Batch experiments were conducted to determine adsorption of Pb, Cu, Zn, Ni, Cr, Fe,

As and NH_4^+ onto the raw CFA, a natural clinker from the Cerrejón coal deposit in Colombia and synthetic zeolites. Using sorbent/AMD ratios of 0.25 g/20 mL and 1 g/20 mL over a period of 24 hours, pH rose only slightly from 1.96 to 2.66 after 1 hour but no breakthrough to alkaline pH was observed using this adsorbent dosage. Adsorption by CFA seemed to partition into two scenarios. In the first, concentrations of the target ion in the final solution were higher than in the original untreated AMD. These ions included NH_4^+, Cr^{3+}, Cu^{2+} and Zn^{2+}. In the second group, CFA adsorbed more ions than it released into solution and final concentrations were lower; As, Zn, Fe and Pb belonged to this group. This study highlights the challenge of using raw CFA in AMD treatment, that is, that although some elemental ions may be attenuated, the concentrations of others may increase.

Column studies provide the opportunity to assess the long-term applicability of CFA treatment of AMD. Pérez-López et al. [23] used column experiments to determine the efficacy of fly ash in attenuating AMD formation from pyritic sludge. They found that while columns filled with pyrite-rich sludge leached drainage that was acidic (pH ~ 2) and rich in sulphate, iron and other metals, those containing sludge and fly ash produced alkaline leachate low in sulphate and lacking iron or other metals. The alkaline fly ash neutralised AMD acidity, thus decreasing metal solubility and increasing their precipitation within the column. In addition, these precipitates formed coatings on pyrite grains, preventing their exposure to oxidising agents thus retarding AMD generation in a process known as microencapsulation [24].

Gitari et al. [10] used column studies to investigate the suitability of CFA and its derivatives as back-fill materials. They therefore designed experiments to measure the AMD treatment efficacy of (i) fresh CFA, (ii) solid residues prepared from exposing CFA to AMD, (iii) blends of the solid residues with varying amounts of fresh CFA (5, 25 and 40%) and (iv) a blend of solid residues with ordinary portland cement (OPC). They found that dissolution of CaO in fly ash and the solid residues, and hydration reactions in OPC were responsible for the initial high pH of the leachates in the different columns. This alkalinity subsequently controlled metal leaching through the formation of aluminium and iron precipitates and the co-precipitation of other elements with these phases. However, the leached fractions of most ions increased with increasing CFA concentrations in the blends, for example, Cr(III) concentrations went from 4.97 to 10.27 μmol L^{-1} and 11.19 μmol L^{-1} as CFA concentrations in solid residue blends increased from 5 to 25% and then to 40%. Sulphates were removed as gypsum ($CaSO_4$) and as such, their attenuation was highly dependent on Ca^{2+} from dissolution of CaO in CFA and OPC. Attenuation of Fe and Al, on the other hand, was pH dependent since the formation of hydroxide precipitates was greater at neutral and basic pH. Subsequent modelling studies using PHREEQ software showed that Fe concentrations were controlled by goethite and amorphous $Fe(OH)_3$ phases while those of Al were controlled by boehmite, basaluminite and gibbsite [25].

In some cases, for example, where AMD passes through dolomitic rocks, the acidity as well as metal and sulphate concentrations may be attenuated, resulting in neutral mine waters. Despite this, sulphate concentrations often remain considerable due to high initial concentrations [26]. Madzivire et al. [27, 28] investigating the use of CFA for sulphate removal found that attenuation was not significant below pH 10. Nevertheless, 60% of sulphate was removed

from the solution at pH above 11 with the addition of gypsum and alumina, and sulphate was removed as ettringite ($Ca_6Al_2(SO_4)_3(OH)_{12}\cdot 26H_2O$). One drawback, however, was that the use of CFA increased the concentrations of B, K, Cr, Mo and Sr in the treated water necessitating the inclusion of an additional treatment step such as adsorption using zeolites. Nevertheless, these studies provide evidence of the applicability of CFA in AMD treatment both in acid neutralisation and metal removal.

Metal removal from AMD proceeds through various mechanisms including precipitation, oxidation, reduction and adsorption. Adsorption efficiency increases with surface area. The large surface areas of CFA splenospheres and cenospheres therefore significantly influence metal adsorption from AMD. Specifically, since surface areas increase with decreasing particle size, smaller particles, particularly nano-sized ones (1–100 nm), likely play a very important role in adsorption of element ions. In fact, CFA has been shown to contain significant quantities of nanoparticles [29, 30] which are enriched in metal ions [31–36]. Despite this, there is a dearth of information regarding the role of CFA nanoparticles during AMD treatment.

This chapter therefore highlights the key role of nanoparticles in remediation effects of CFA. Using Fe oxy(hydroxides), Ti dioxides and carbon nanotubes phases known to be abundant in CFA [29, 37–39], we illustrate the likely effect of nanoparticle-based processes on observed metal removal efficiencies of CFA.

2. Nanomaterials in CFA

2.1. Properties of nanomaterials

Consider a crystal of iron or titanium oxide. In the bulk of the crystal, Fe or Ti ions are surrounded (coordinated) by six nearest-neighbour oxygen atoms, an arrangement that balances the electric charge of anions and metal atoms. However, when the bulk is divided into smaller particles, new surfaces are created and the spatial configuration of the bulk is lost. This leads to an increase in surface energies which the newly exposed atoms on the surface attempt to dissipate by re-organising, for example, 'dangling' oxygen atoms may form bridged pairs. Such surface reconstructions result in particles with considerably different properties from those of the bulk material [40, 41].

In fact, many of the unique characteristics of nanomaterials (NMs) are the result of size-dependent surface properties. There is evidence that properties, including crystalline habit, magnetism and colour, change with particle size [42]. In addition, the proportion of atoms located at or near particle surfaces increases as particle size decreases. The extra surface charge increases particle reactivity, hence smaller particles are more reactive than bulk counterparts [43, 44]. Brown et al. [45] also showed that the larger number of edge and corner binding sites as well as the wide variety of defects on the surfaces of NMs (**Figure 1**) is responsible for increased reactivity at the nano-scale. Adsorption of ions from surrounding media may be a means to reduce surface energy and regain particle stability. Thus, NMs are excellent adsorbents due to their large surface areas and abundant, highly reactive surface sorption sites.

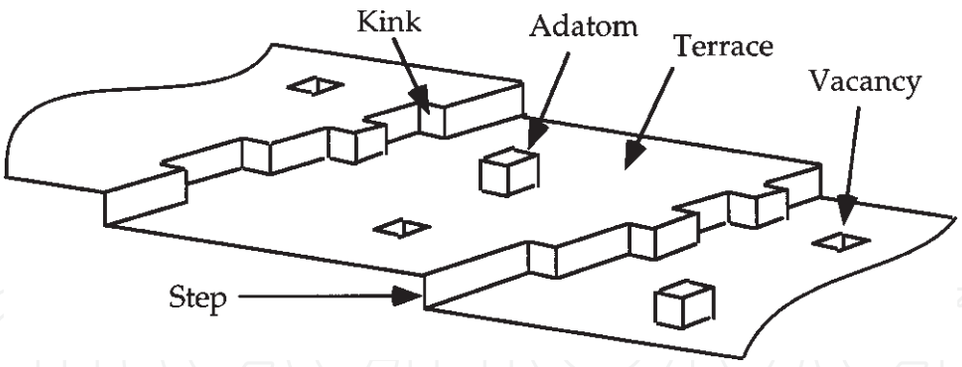

Figure 1. A model of possible defects on single-crystal surface [45].

2.2. Evidence of nanomaterials in CFA

Advancements in various microscopic and spectroscopic techniques have facilitated the identification of nano-sized materials in CFA. By combining transmission and scanning electron microscopy, as well as atomic force microscopy and X-ray diffraction (XRD) for instance, Dwivedi et al. [46] found that CFA from Harduaganj in Aligard, India, contained spherical particles with sizes ranging from 11 to 25 nm. In another study, high resolution transmission electron microscopy (HR-TEM) and energy-dispersive X-ray spectroscopy (EDS) revealed the presence of 10–100 nm hematite and yavapaiite ($KFe(SO_4)_2$) nanoparticles in CFA from a power plant in Santa Catarina state in Brazil [34].

Ribeiro et al. [32] coupled EDS with field-scanning electron microscopy (FE-SEM) and HR-TEM to characterise CFA from an anthracite-burning thermal power plant in, Porto, Portugal. Besides the larger cenospheres (~ 100 μm), ultrafine glassy spheres (~ 100 nm) as well as carbonaceous nanospheres (~ 50 nm) and nanotubes (0.1–32 nm in diameter and 8–59 μm in length) were identified in the CFA (**Figure 2**).

Fe was present as maghemite, hematite and magnetite or as sulphates, that is, schwertmannite and jarosite and titanium as anatase and rutile. Quartz nanoparticles were also identified occurring discretely or embedded in amorphous phases, for example, glass and nano-spherules rich in Al, Si, Ti, K, Mg and Fe were frequently observed embedded in carbonaceous matrices. Indeed, these inorganic phases are often found encapsulated by carbonaceous matter although Wilcox et al. [47] showed that this encapsulation may be a factor of the amount of carbon in feed coal. Comparing CFA from pure high sulphur-high Fe bituminous coal and a blend consisting of 70% of this high sulphur-high Fe coal and 30% of a low sulphur-high CaO coal, these authors found that unlike CFA from the pure coal, inorganic particles in CFA from the blend did not contain any carbon on their surface (**Figure 3**). The composition of CFA particles therefore depends, to some extent, on the nature of feed coal burned; with the amount of carbon rather than the rank of coal determining coal deposition on CFA particles.

As a final example, let us consider the ultrafines (particles < 100 nm) in CFA from US coals examined by Chen et al. [48]. These nanoparticles were found to have distinctly different morphologies, compositions and microstructures (**Figure 4**). In addition, CFA from a bituminous

http://dx.doi.org/10.5772/intechopen.69426

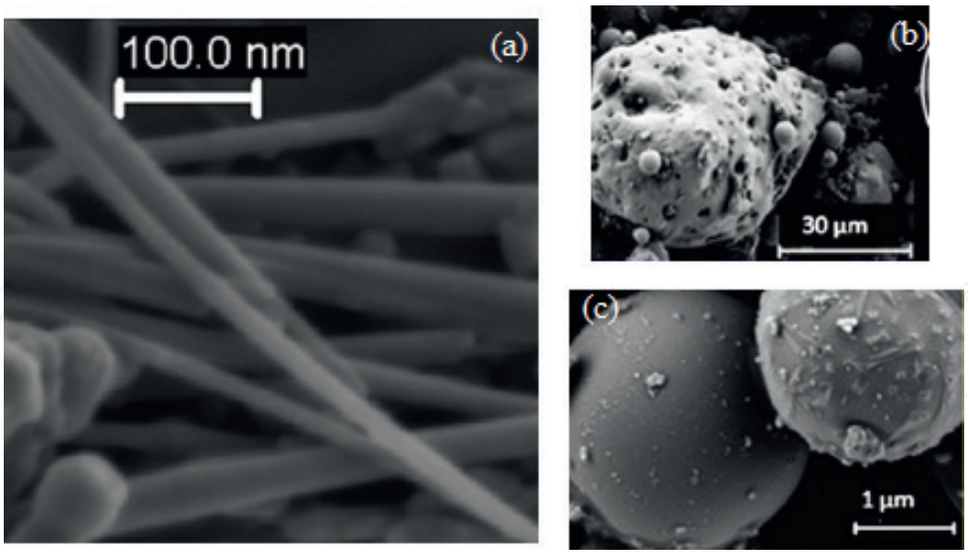

Figure 2. Carbon nanotubes (a) and carbonaceous spheres (b) and (c) in CFA from anthracite coal [32].

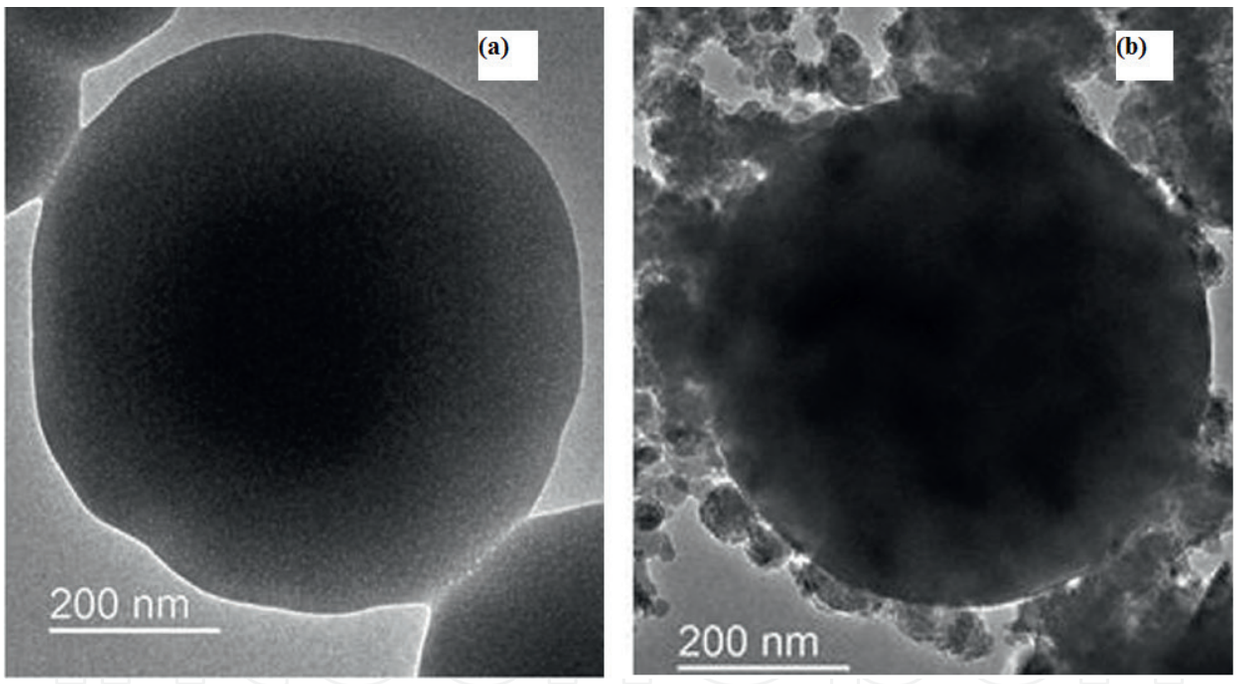

Figure 3. TEM images of (a) particles from the CFA blend. Note the absence of carbon deposits on the surface. (b) CFA particles from combustion of pure high sulphur-high Fe bituminous coal [47].

coal was rich in crystalline phases of Fe, Ti and Al as small as 10 nm while a low-rank CFA was rich in aggregates of alkaline-earth elements in the form of sulphates, silicates and phosphates.

Nano-scale unburned carbon was present as soot aggregates ranging in size from 100 to 1000 although aggregated smaller than 100 nm were also present. Their morphology was similar to that of soot aggregates from diesel engine exhausts. Importantly, these aggregates are made up of 20–50 nm primary particles arranged in an onion-like structure (**Figure 5**). Their formation,

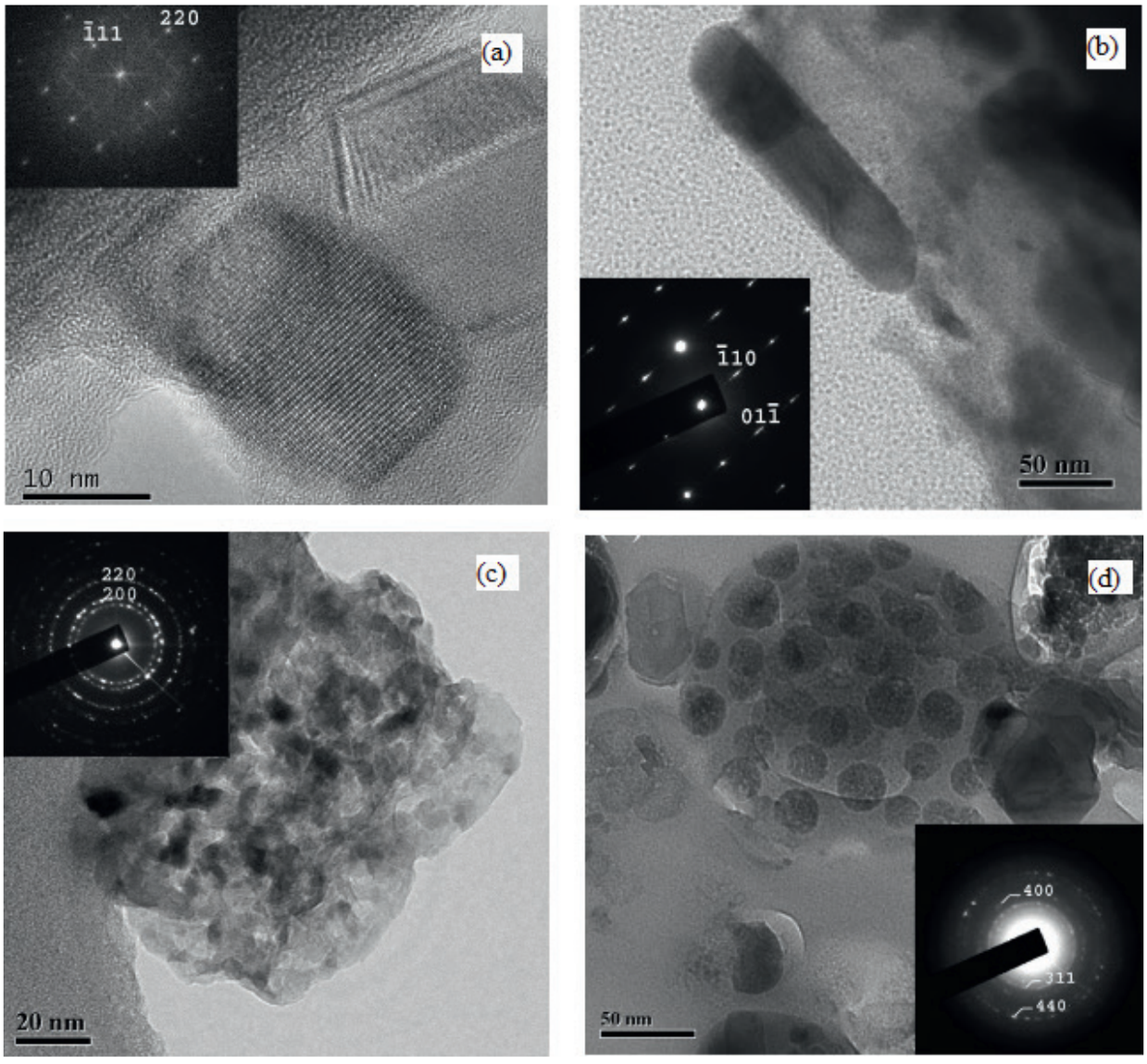

Figure 4. (a) Magnetite nanocrystalline particles, (b) a rod-like rutile particle, (c) a lime particle containing 5–10 nm nanocrystallites and (d) a cluster of $FeAl_2O_4$ particles on an amorphous silica sphere. Inserts in (a) and (b) are fast Fourier transforms (FFT) of the images and those in (c) and (d) are selected area electron diffraction (SAED) patterns [48].

as we will see shortly, likely involves sudden quenching and homogenous condensation of refractory carbon-rich species in the combustion atmosphere.

2.3. Mechanisms of nanomaterial formation in CFA

Having confirmed their presence, let us now briefly consider the mechanisms that lead to the formation of nano-sized materials in CFA. While several mechanisms are responsible for particulate formation in CFA, the formation of nanoparticles is dominated by (i) the release of organically bound metals during coal volatilisation and (ii) vaporisation and subsequent condensation and aggregation of such elements [30, 49]. Nanoparticles in CFA may be categorised as either organic or inorganic and are formed through two separate pathways as illustrated in **Figure 6**.

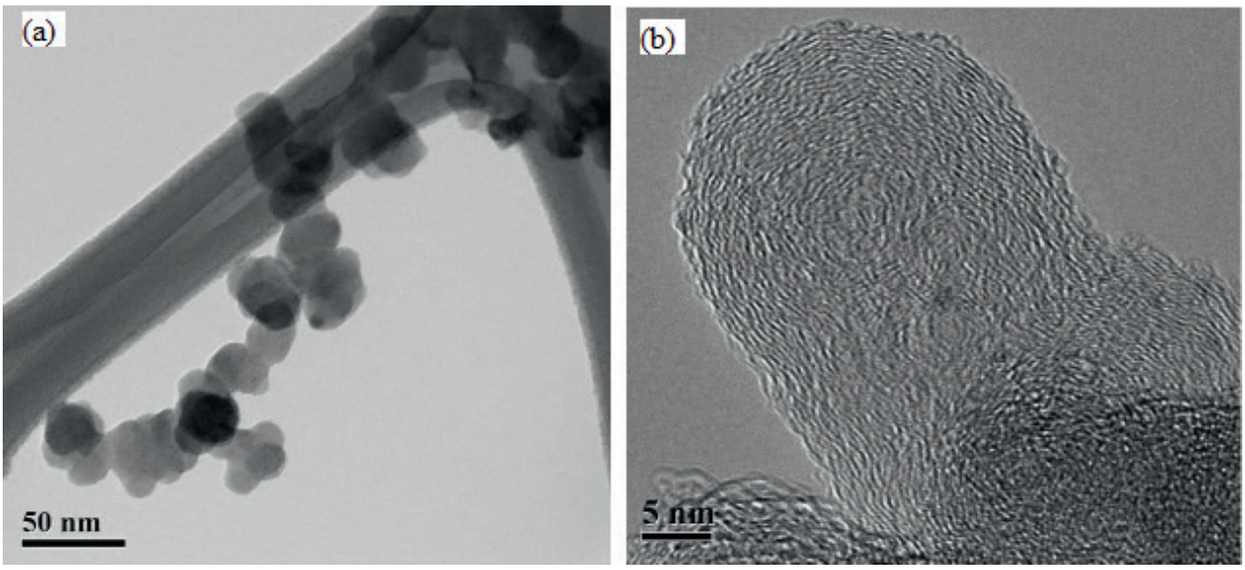

Figure 5. (a) Coal fly ash soot aggregates with chain-like branching structure, (b) concentric stacking of graphitic layers making up soot particles [48].

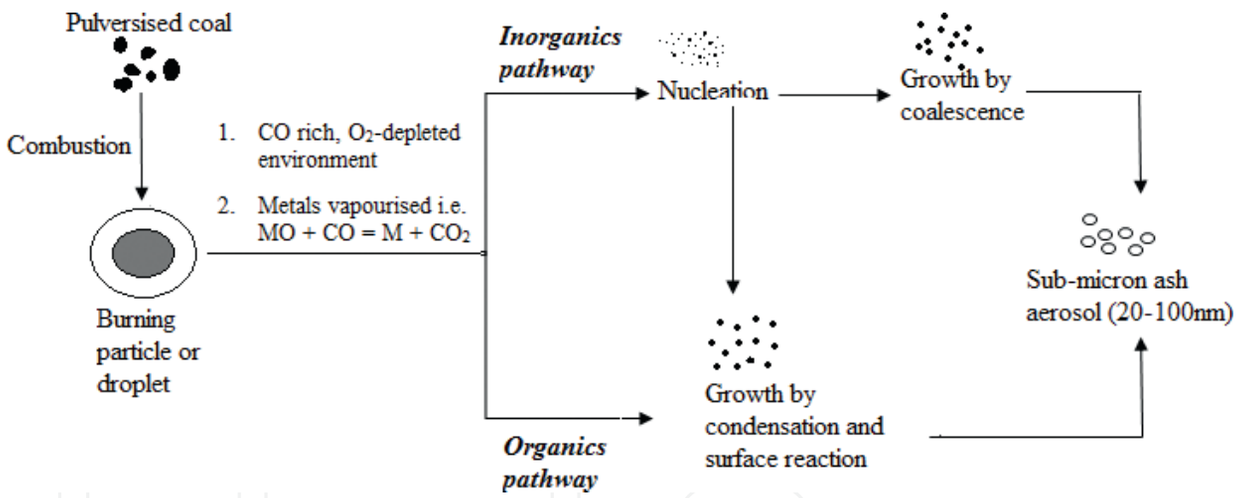

Figure 6. Formation of nanomaterials in coal fly ash.

The formation of inorganic particles occurs through nucleation, also known as homogeneous condensation of flame-volatilised species [50–54], for example, SiO_2, CaO and Fe_2O_3. The main features of this process were outlined by Nelson [51] thus:

(i) The highly reducing conditions existing within coal chars during combustion reduce refractory oxides to more volatile sub-oxides or elements, for example, for Si:

$$SiO_2(s) + CO\ (g) \rightarrow SiO\ (g) + CO_2(g) \quad (1)$$

(ii) As the volatile species move away from the particle to the bulk gas, they are re-oxidised due to the higher O_2 concentrations

$$SiO(g) + O_2(g) \rightarrow SiO_2(g) + O(g) \quad (2)$$

(iii) Provided the vapour pressure of the oxide exceeds the saturated vapour pressure, spontaneous condensation will occur and nuclei will form. Particle growth then proceeds via coalescence. Particle growth may also be the result of heterogeneous condensation, that is, condensation of other species upon these particles. This happens mostly from species that vaporise but whose concentrations are not sufficient for homogenous condensation.

Organic particles, or soot, form under fuel-rich conditions where hydrocarbon fragments have greater chances of colliding and growing instead of being oxidised to CO, CO_2, H_2 and H_2O. Their formation involves chemical reactions that produce clusters of increasing molecular weight to the point where these clusters are visible as particles [30]. The formation of the first aromatic ring, usually benzene, is considered one of the critical steps in soot formation. Benzene rings then go on to form polycyclic aromatic hydrocarbons which increase in molecular weight to soot particles (**Figure 7**).

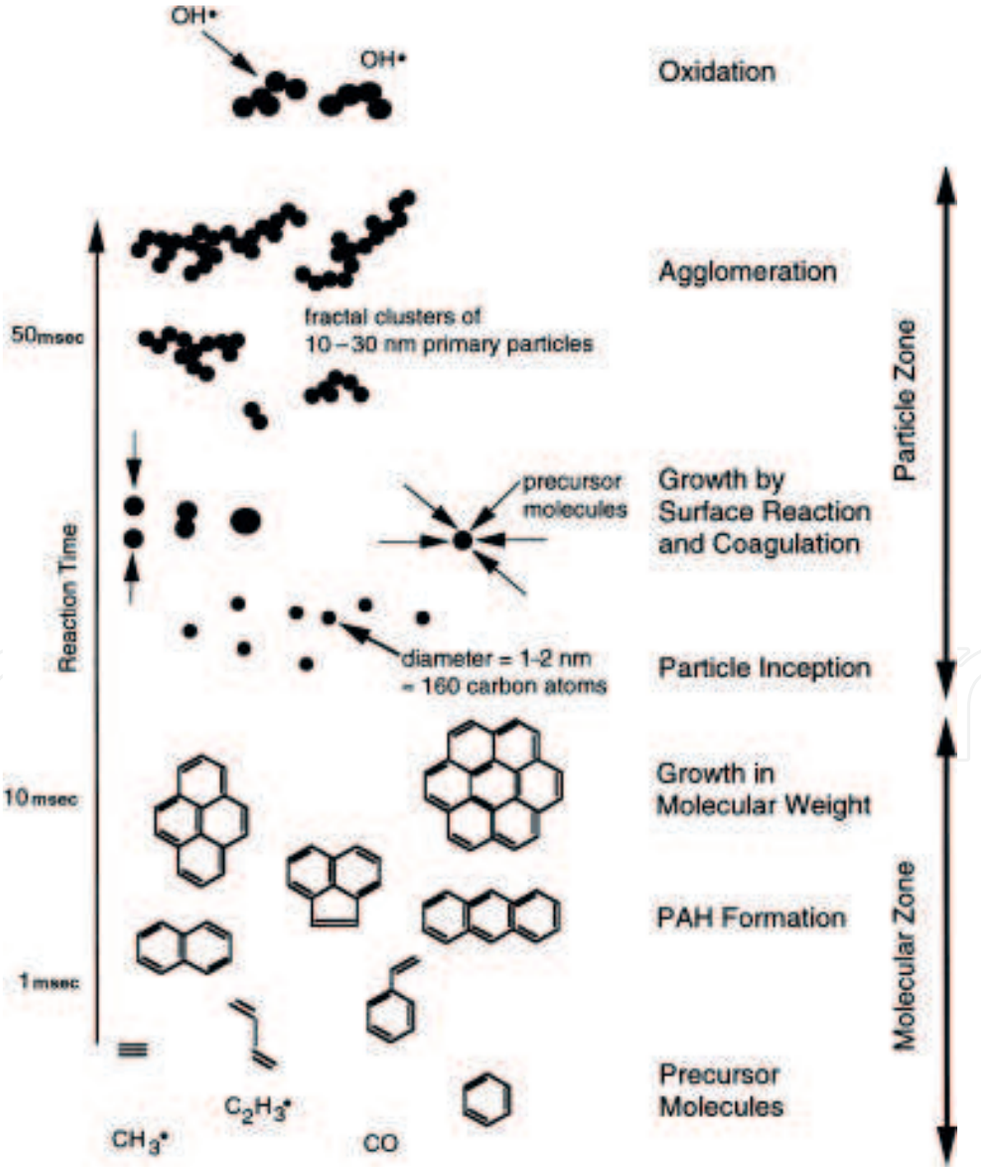

Figure 7. Chemical and physical processes involved in the formation of soot particles [30].

Other factors influencing formation of both organic and inorganic particles include (i) temperature [39, 55], (ii) gas composition [56–59] and coal rank [47, 58, 60]. Particle formation is enhanced at higher temperatures due to increased mineral vaporisation and environments with low oxygen to fuel stoichiometry produce less ultrafines [57]. In addition, Wen et al. [61] recently reported that combustion under N_2 resulted in production of more particulates than combustion in CO_2. The effect of coal rank, on the other hand, is multifarious and can be summarised as follows:

(i) The higher char reactivity of lower rank coals favours the formation of nanoparticles because of the higher combustion temperatures of these chars [62];

(ii) The reducing atmosphere produced by carbon combustion at high temperatures increases ash vaporisation [59];

(iii) Low-rank coals have high concentrations of alkaline-earth metals which supress the vaporisation of silica by reacting with it to form less volatile silicates. This results in nanoparticles from combustion of lignite being mostly MgO and CaO, and SiO_2 nanoparticles being significant only in bituminous coal [59].

3. Metal binding by nanomaterials and larger CFA particles

CFA contains nanomaterials of various parent minerals and elements. These include (i) iron oxides which comprise a large fraction of the inorganic nanoparticles in CFA occurring as pyrite, pyrrhotite, magnetite, hematite, jarosite, goethite and yavapaiite [32, 34, 63–65] and (ii) carbon nanomaterials, for example, single- or multi-walled nanotubes [29, 32, 46, 47].

Both organic and inorganic nanoparticles in fly ash are associated with higher concentrations of metal ions in CFA than larger particles. In fact, it has been known since the work of Davison et al. [52] that element enrichment in CFA is inversely related to particle size. These authors found that concentrations of Pb, Ti, Sb, Cd, Se, As, Ni, Cr and Zn increased with decreasing CFA particle size and that particles with aerodynamic diameters >40 μm, for example, had Pb loadings up to 90 $\mu g\ g^{-1}$ while those with diameters below 5 μm had loadings of up to 980 $\mu g\ g^{-1}$. Positing at first that this observation was due to the fragmentation of pyritic inclusions in the coal, they later inclined to the homogenous and heterogeneous condensation hypotheses explained above. Later, Linak et al. [66] also reported up to 50 times enrichment of S, Cl, Na, K, V and P in ultrafines; confirming that the smaller the particles, the higher the concentrations of metals sorbed onto their surfaces.

Yi et al. [39] studied the relative distributions of trace elements in bottom ash, fly ash and flue gas. They found that except Hg whose concentration was highest in flue gas, all other elements (As, Cd, Cr, Cu, Al, V, Zn, Mn and Fe) were enriched in fly ash relative to bottom ash (**Figure 8**). Similar results were reported for various Indian fly ashes [37, 38, 67]. Hg, although occurring in high concentrations in flue gases, is also bound to a considerable extent to inorganic fractions as we will see later, and to the organic fraction of CFA by carboxylic acid functional groups [29].

For some time, this phenomenon (element enrichment in nanoparticles) was thought of as being purely the result of the greater surface areas available for adsorption in smaller particles

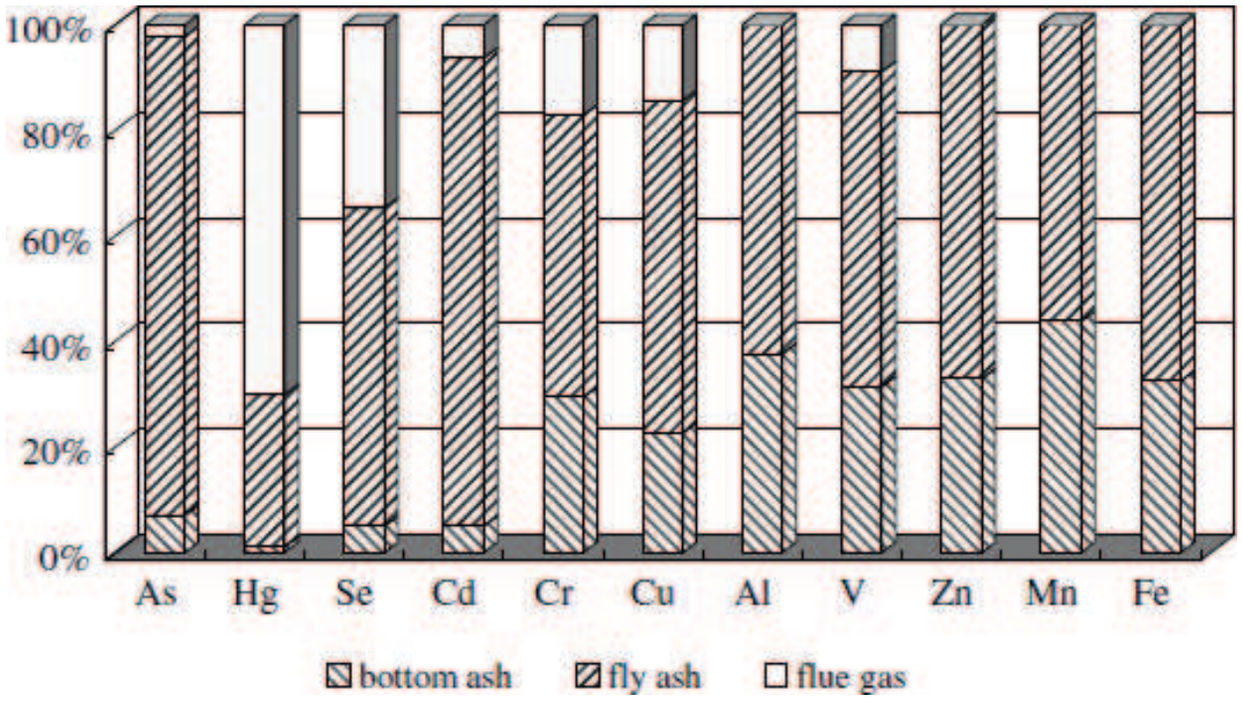

Figure 8. Relative distributions of trace elements in bottom ash, fly ash and flue gas from a coal boiler [39].

[52]. However, later geochemical investigations showed that surface features of these particles played a significant role. Nanoparticle binding of metal ions has been shown to involve faster kinetics [68–70], speciation transformations of the adsorbed species [71] and greater affinity for metal ions [69]. In addition, there is evidence that some of these phenomena, specifically higher reaction rates, are due to surface defects. Junta and Hochella [72] found that in the oxidation of Mn^{2+} to Mn^{3+} at hematite nanoparticle surfaces, steps were the most reactive sites for initiating the adsorption-oxidation reaction. Later, Madden and Hochella [68] found that this oxidation process was up to 1.5 orders of magnitude faster on 7.3 nm particles than on 37 nm particles largely due to changes in the electronic structure of hematite. As its particles get smaller, the Lewis basicity of the surface oxygen increased, decreasing the redox potential of adsorbed Mn^{2+} and making the oxidation reaction more favourable.

The nature of binding sites at the nano-scale has also been invoked to explain changes in metal adsorption. Greater binding of Cu^{2+} ions to 7 nm hematite particles, relative to the larger 25 and 88 nm counterparts was due to the greater number, in the smallest particles, of distorted octahedral sites in which Cu^{2+} ions are better stabilised [69]. This hypothesis correlates with the observations of the association of Hg with Fe-rich sites in nano-sized CFA, but not in larger particles [29]. Such unique material properties occurring at the nano-scale properties likely account for the metal-nanoparticle interactions observed in various investigations cited above.

Having examined the relationship between metal ions and nano-sized fractions of CFA and shown that these particles bind larger fractions of metals than micron-sized particles, let us now examine evidence that this phenomenon carries over when CFA is used for remediation

of contaminated water, that is, that the nano-sized fraction is still responsible for a greater fraction of the metal removal observed. Synchrotron-based X-ray fluorescence was used to study the adsorption of Hg from flue gas by fly ash from a Kentucky utility [29]. The bulk ash (20 nm–10 μm in diameter) was largely amorphous with only quartz and hematite as crystalline phases. The fine ash had an average particle size of < 100 nm and comprised of more crystalline phases and some cementitious phases, for example, syngenite ($K_2Ca(SO_4)_2 \cdot H_2O$), glauberite ($Na_2Ca(SO_4)_2$) and picromerite ($K_2Mg(SO_4)_2$). A summary of Hg concentrations of the two classes of ash and fine ash before and after exposure to flue gas is presented in **Table 2**.

The 100 nm fraction represented only 0.01% of the total fly ash content. Nevertheless, it is clear from these data that despite already containing greater Hg concentrations before the exposure reaction, nano-sized CFA particles dominated Hg uptake from the flue gases.

Mercury was bound to hematite by bidentate inner-sphere complexes. The nature of binding is an important consideration because of its role in desorption processes as inner-sphere complexes are known to be more stable and less prone to desorption than outer-sphere complexes [43]. Using extended X-ray absorption fine structure (EXAFS) spectroscopy, Ha et al. [73] showed that Zn(II) surface complexes on 10.5 nm hematite particles were more strongly held than those adsorbed to 550 nm particles. As a result, only 10–15% of Zn^{2+} ions were desorbed from the 10.5 nm particles where they were held as inner-sphere complexes but up to 40% were lost from the larger particles where Zn^{2+} ions were held in outer-sphere complexes. This highlights the fact that nanoparticles bind metal ions differently and that this is likely to influence the long-term effectiveness of remediation activity.

	Hg concentration before flue gas exposure	Hg concentration after flue gas exposure
Bulk ash	11 ± 0.8 ppb	161 ± 4 ppb
Fine ash	100 ± 6 ppb	610 ± 20 ppb

Table 2. Hg concentrations in bulk and nano-sized particles before and after exposure to flue gases.

4. Directions for future research

As stated at the beginning of this chapter, despite the numerous studies showing the efficiency of CFA in treatment of AMD, none of those we have come across specifically describe the role of nanomaterials in this process. Nevertheless, the evidence systematically synthesised in this chapter has shown that nano-scale materials likely account for most of the remedial action of CFA. Despite the cost effectiveness and efficiency of CFA at remediation, potential secondary contamination by other must always be addressed before its application in the field. Future research should investigate the potential role of photocatalytic nanoparticles in CFA, in pollutant transformation.

Author details

Anita Etale[1]*, Nikita T. Tavengwa[2] and Vusumzi E. Pakade[3]

*Address all correspondence to: aetale@gmail.com

1 ETH Zurich, Institute for Environmental Decisions (IED), Consumer Behaviour, Universitätstrasse, Zurich, Switzerland

2 Department of Chemistry, School of Mathematical and Natural Sciences, University of Venda, Thohoyandou, South Africa

3 Department of Chemistry, Vaal University of Technology, Vanderbijlpark, South Africa

References

[1] International Energy Agency, Key World Energy Statistics; 2016, 80pp

[2] Ahmaruzzaman M. A review on the utilization of fly ash. Progress in Energy and Combustion Science. 2010;**36**:327-363

[3] Blissett RS, Rowson NA. A review of the multi-component utilisation of coal fly ash. Fuel. 2012;**97**:1-23

[4] Temuujin J, Minjigmaa A, Davaabal B, Bayarzul U, Ankhtuya A, Jadambaa Ts, MacKenzie KJD. Utilization of radioactive high-calcium Mongolian fly ash for the preparation of alkali-activated geopolymers for safe use as construction materials. Ceramics International. 2014;**40**:16475-16483

[5] Durand JF. The impact of gold mining on the Witwatersrand on the rivers and karst system of Gauteng and North West Province, South Africa. Journal of African Earth Sciences. 2012;**68**:24-43

[6] Nieto JM, Sarmiento AM, Olías M, Canovas CR, Riba I, Kalman J, Delvalls TA. Acid mine drainage pollution in the Tinto and Odiel rivers (Iberian Pyrite Belt, SW Spain) and bioavailability of the transported metals to the Huelva Estuary. Environment International. 2007;**33**:445-455

[7] Singer PC, Stumm W. Acidic mine drainage: The rate-determining step. Science. 1970; **167**:1121-1123

[8] Byrne P, Wood PJ, Reid I. The impairment of river systems by metal mine contamination: A review including remediation options. Critical Reviews in Environmental Science and Technology. 2012;**42**:2017-2077

[9] Cho H, Oh D, Kim K. A study on removal characteristics of heavy metals from aqueous solution by fly ash. Journal of Hazardous Materials. 2005;**127**:187-195

[10] Gitari WM, Petrik LF, Etchebers O, Key DL, Iwuoha E, Okujeni C. Passive neutralisation of acid mine drainage by fly ash and its derivatives: A column leaching study. Fuel. 2008;**87**:1637-1650

[11] Koshy N, Singh DN. Fly ash zeolites for water treatment applications. Journal of Environmental Chemical Engineering. 2016;**4**:1460-1472

[12] Belviso C, Cavalcante F Di Gennaro S, Lettino A, Palma A, Ragone P, Fiore S. Removal of Mn from aqueous solution using fly ash and its hydrothermal synthetic zeolite. Journal of Environmental Management. 2014;**137**:16-22

[13] Visa M. Synthesis and characterization of new zeolite materials obtained from fly ash for heavy metals removal in advanced wastewater treatment. Powder Technology. 2016;**294**:338-347

[14] Attari M, Bukhari SS, Kazemian H, Rohani S. A low-cost adsorbent from coal fly ash for mercury removal from industrial wastewater. Journal of Environmental Chemical Engineering. 2017;**5**:391-399

[15] Ogata F, Iwata Y, Kawasaki N. Properties of novel adsorbent produced by hydrothermal treatment of waste fly ash in alkaline solution and its capability for adsorption of tungsten from aqueous solution. Journal of Environmental Chemical Engineering. 2015;**3**:333-338

[16] Sočo E, Kalembkiewicz J. Removal of Copper(II) and Zinc(II) ions from aqueous solution by chemical treatment of coal fly ash. Croatica Chemica Acta. 2015;**88**:267-279

[17] Pizarro J, Castillo X, Jara S, Ortiz C, Navarro P, Cid H, Rioseco H, Barros D, Belzile N. Adsorption of Cu^{2+} on coal fly ash modified with functionalized mesoporous silica. Fuel. 2015;**156**:96-102

[18] Kim HJ, Joshi MK, Pant HR, Kim JH, Lee E, Kim CS. One-pot hydrothermal synthesis of multifunctional Ag/ZnO/fly ash nanocomposite. Colloids Surfaces A: Physicochemical and Engineering Aspects. 2015;**469**:256-262

[19] Ökte AN, Karamanis D. A novel photoresponsive ZnO-flyash nanocomposite for environmental and energy applications. Applied Catalysis B Environmental. 2013;**142-143**: 538-552

[20] Qi G, Lei X, Li L, Yuan C, Sun Y, Chen J. Chen J, Wang Y, Hao J. Preparation and evaluation of a mesoporous calcium-silicate material (MCSM) from coal fly ash for removal of Co(II) from wastewater. Chemical Engineering Journal. 2015;**279**:777-787

[21] Papandreou AD, Stournaras CJ, Panias D, Paspaliaris I. Adsorption of Pb(II), Zn(II) and Cr(III) on coal fly ash porous pellets. Minerals Engineering. 2011;**24**:1495-1501

[22] Ríos CA, Williams CD, Roberts CL. Removal of heavy metals from acid mine drainage (AMD) using coal fly ash, natural clinker and synthetic zeolites. Journal of Hazardous Materials. 2008;**156**:23-35

[23] Pérez-López R, Nieto JM, de Almodóvar GR. Utilization of fly ash to improve the quality of the acid mine drainage generated by oxidation of a sulphide-rich mining waste: Column experiments. Chemosphere. 2007;**67**:1637-1646

[24] Evangelou VP. Pyrite chemistry: The key for abatement of acid mine drainage. In: Geller W, Klapper H, Salomons W, editors. Acidic Min. Lakes Acid Mine Drainage, Limnol. Reclam. 1st ed. Berlin Heidelberg: Springer-Verlag; 1998. pp. 197-222

[25] Gitari WM, Petrik LF, Etchebers O, Key DL, Okujeni C. Utilization of fly ash for treatment of coal mines wastewater: Solubility controls on major inorganic contaminants. Fuel. 2008;**87**:2450-2462

[26] Banks D, Younger PL, Egil RA, Sheila RI. Mine-water chemistry: The good, the bad and the ugly. Environmental Geology. 1997;**32**:157-174

[27] Madzivire G, Petrik LF, Gitari WM, Ojumu TV, Balfour G. Application of coal fly ash to circumneutral mine waters for the removal of sulphates as gypsum and ettringite. Minerals Engineering. 2010;**23**:252-257

[28] Madzivire G, Gitari WM, Vadapalli VRK, Ojumu TV, Petrik LF. Fate of sulphate removed during the treatment of circumneutral mine water and acid mine drainage with coal fly ash: Modelling and experimental approach. Minerals Engineering. 2011;**24**:1467-1477

[29] Jew AD, Rupp EC, Geatches DL, Jung JE, Farfan G, Bahet L, Hower JC, Brown Jr GD, Wilcox J. Mercury interaction with the fine fraction of coal-combustion fly ash in a simulated coal power plant flue gas stream. Energy and Fuels. 2015;**29**:6025-6038

[30] Lighty JS, Veranth JM, Sarofim AF. Combustion aerosols: Factors governing their size and composition and implications to human health. Journal of the Air & Waste Management Association. 2000;**50**:1565-1618

[31] Chen Y, Shah N, Huggins FE, Huffman GP, Dozier A. Characterization of ultrafine coal fly ash particles by energy-filtered TEM. Journal of Microscopy. 2005;**217**:225-234

[32] Ribeiro J, DaBoit, K Flores D, Kronbauer MA, Silva LFO. Extensive FE-SEM/EDS, HR-TEM/EDS and ToF-SIMS studies of micron- to nano-particles in anthracite fly ash. Science of the Total Environment. 2013;**452-453**:98-107

[33] Silva LFO, Oliveira MLS, Neace ER, O'Keefe JMK, Henke KR, Hower JC. Nanominerals and ultrafine particles in sublimates from the Ruth Mullins coal fire, Perry County, Eastern Kentucky, USA. International Journal of Coal Geology. 2011;**85**:237-245

[34] Silva LFO, Moreno T, Querol X. An introductory TEM study of Fe-nanominerals within coal fly ash. Science of the Total Environment. 2009;**407**:4972-4974

[35] Saikia J, Narzary B, Roy S, Bordoloi M, Saikia P, Saikia BK. Nanominerals, fullerene aggregates, and hazardous elements in coal and coal combustion-generated aerosols: An environmental and toxicological assessment. Chemosphere. 2016;**164**:84-91

[36] Ribeiro J, Flores D, Ward CR, Silva LFO. Identification of nanominerals and nanoparticles in burning coal waste piles from Portugal. Science of the Total Environment. 2010;**408**:6032-6041

[37] Bhanarkar AD, Gavane AG, Tajne DS, Tamhane SM, Nema P. Composition and size distribution of particules emissions from a coal-fired power plant in India. Fuel. 2008;**87**: 2095-2101

[38] Reddy MS, Basha S, Joshi HV, Jha B. Evaluation of the emission characteristics of trace metals from coal and fuel oil fired power plants and their fate during combustion. Jurnal of Hazardous Materials. 2005;**123**:242-249

[39] Yi H, Hao J, Duan L, Tang X, Ning P, Li X. Fine particle and trace element emissions from an anthracite coal-fired power plant equipped with a bag-house in China. Fuel. 2008;**87**:2050-2057

[40] Gilbert B. Nanoparticles: Strained and stiff. Science. 2004;**305**:651-654

[41] Banfield JF, Zhang H. Nanoparticles in the environment. Reviews in Mineralogy and Geochemistry. 2001;**44**:1-51. DOI: 10.2138/rmg.2001.44.01

[42] Waychunas GA, Zhang H. Structure, chemistry, and properties of mineral nanoparticles. Elements. 2008;**4**:381-388. DOI: 10.2113/gselements.4.6.381

[43] Brown GE, Calas G. Environmental mineralogy – Understanding element behavior in ecosystems. Comptes Rendus Geoscience. 2011;**343**:90-112

[44] Hochella Jr MF, Lower SK, Maurice PA, Penn RL, Sahai N, Sparks DL, Twining BS. Nanominerals, mineral nanoparticles, and earth systems. Science. 2008;**80**:1631-1636

[45] Brown GE, Henrich VE, Casey WH, Clark DL, Eggleston C, Felmy A, Goodman DW, Grätzel M, Maciel G, McCarthy MI, Nealson KH, Sverjensky DA, Toney MF, Zachara JM. Metal oxide surfaces and their interactions with aqueous solutions and microbial organisms. Chemical Reviews. 1999;**99**:77-174

[46] Dwivedi S, Saquib Q, Al-Khedhairy AA, Ali A-YS, Musarrat J. Characterization of coal fly ash nanoparticles and induced oxidative DNA damage in human peripheral blood mononuclear cells. Science of the Total Environment. 2012;**437**:331-338

[47] Wilcox J, Wang B, Rupp E, Taggart R, Hsu-Kim H, Oliveira MLS, Cutruneo CMNL, Taffarel S, Silva LFO, Hopps SD, Thomas GA, Hower JC. Observations and assessment of fly ashes from high-sulfur bituminous coals and blends of high-sulfur bituminous and subbituminous coals: Environmental processes recorded at the macro- and nanometer scale. Energy and Fuels. 2015;**29**:7168-7177

[48] Chen Y, Shah N, Huggins FE, Huffman GP. Transmission electron microscopy investigation of ultrafine coal fly ash particles. Environmental Science & Technology. 2005;**39**: 1144-1151

[49] Niu Y, Wang S, Shaddix CR, Hui S. Kinetic modeling of the formation and growth of inorganic nano-particles during pulverized coal char combustion in O_2/N_2 and O_2/CO_2 atmospheres. Combustion and Flame. 2016;**173**:195-207

[50] Linak WP, Wendt JOL. Toxic metal emissions from incineration: Mechanisms and control. Progress in Energy and Combustion Science. 1993;**19**:145-185. DOI: 10.1016/0360-1285(93)90014-6

[51] Nelson PF. Trace metal emissions in fine particles from coal combustion. Energy and Fuels. 2007;**21**:477-484

[52] Davison RL, Natusch DFS, Wallace JR, Evans CA. Trace elements in fly ash. Dependence of concentration on particle size. Environmental Science & Technology. 1974;**8**:1107-1113

[53] Galbreath KC, Toman DL, Zygarlicke CJ, Pavlish JH. Trace element partitioning and transformations during combustion of bituminous and subbituminous U.S. coals in a 7-kW combustion system. Energy and Fuels. 2000;**14**:1265-1279

[54] Markowski GR, Filby R. Trace element concentration as a function of particle size in fly ash from a pulverized coal utility boiler. Environmental Science & Technology. 1985; **19**:796-804

[55] Fix G, Seames W, Mann M, Benson S, Miller D. The effect of combustion temperature on coal ash fine-fragmentation mode formation mechanisms. Fuel. 2013;**113**:140-147

[56] Chen Y, Wang G, Sheng C. Comparison of particle size evolution during pulverized coal combustion in O_2/CO_2 and O_2/N_2 atmospheres. Energy and Fuels. 2014;**28**:136-145

[57] Fix G, Seames WS, Mann MD, Benson SA, Miller DJ. The effect of oxygen-to-fuel stoichiometry on coal ash fine-fragmentation mode formation mechanisms. Fuel Processing Technology. 2011;**92**:793-800

[58] Kazanc F, Levendis YA. Physical properties of particulate matter emitted from combustion of coals of various ranks in O_2/N_2 and O_2/CO_2 environments. Energy and Fuels. 2012;**26**:7127-7139

[59] Neville M, Quann RJ, Haynes BS, Sarofim F. Vaporization and condensation of mineral matter during pulversized coal combustion. Symposium (International) on Combustion. 1981;**18**:1267-1274

[60] Kazanc F, Levendis YA, Maffei T. Chemical composition of submicrometer particulate matter (PM_1) emitted from combustion of coals of various ranks in O_2/N_2 and O_2/CO_2 environments. Energy and Fuels. 2013;**27**:4984-4998

[61] Wen C, Fan B, Wang W, Zeng X, Yu G, Lv W, Minghou X. Preliminary research on the effects of coal devolatilization and char combustion processes on the emission of particulate matter during lignite combustion under air and oxy-fuel conditions. Energy and Fuels. 2017;**31**:24-230

[62] Wen C, Xu M, Yu D, Sheng C, Wu H, Zhang P, et al. PM_{10} formation during the combustion of N_2-char and CO_2-char of Chinese coals. Proceedings of the Combustion Institute. 2013;**34**:2383-2392

[63] Oliveira MLS, Marostega F, Taffarel SR, Saikia BK, Waanders FB, DaBoit K, Baruach BP, Silva LFO. Nano-mineralogical investigation of coal and fly ashes from coal-based captive power plant (India): An introduction of occupational health hazards. Science of the Total Environment. 2014;**468-469**:1128-1137

[64] Martinello K, Oliveira MLS, Molossi FA, Ramos CG, Teixeira EC, Kautzmann RM. Silver LFO. Direct identification of hazardous elements in ultra-fine and nanominerals from coal fly ash produced during diesel co-firing. Science of the Total Environment. 2014;**470-471**:444-452

[65] Saikia BK, Ward CR, Oliveira MLS, Hower JC, Baruah BP, Braga M, Silver LF Geochemistry and nano-mineralogy of two medium-sulfur northeast Indian coals. International Journal of Coal Geology. 2014;**121**:26-34

[66] Linak WP, Yoo JI, Wasson SJ, Zhu W, Wendt JOL, Huggins FE, Chen Y, Shah N, Huffman GP, Gilmour MI. Ultrafine ash aerosols from coal combustion: Characterization and health effects. Proceedings of the Combustion Institute. 2007;**31**(2):1929-1937

[67] Bhangare RC, Ajmal PY, Sahu SK, Pandit GG, Puranik VD. Distribution of trace elements in coal and combustion residues from five thermal power plants in India. International Journal of Coal Geology. 2011;**86**:349-356

[68] Madden A, Hochella M. A test of geochemical reactivity as a function of mineral size: Manganese oxidation promoted by hematite nanoparticles. Geochimica et Cosmochimica Acta. 2005;**69**:389-398

[69] Madden AS, Hochella MF, Luxton TP. Insights for size-dependent reactivity of hematite nanomineral surfaces through Cu^{2+} sorption. Geochimica et Cosmochimica Acta. 2006;**70**:4095-4104

[70] Waychunas GA, Kim CS, Banfield JF. Nanoparticulate iron oxide minerals in soils and sediments: Unique properties and contaminant scavenging mechanisms. Journal of Nanoparticle Research. 2005;**7**:409-433

[71] Weaver RM, Hochella MF, Ilton ES. Dynamic processes occurring at the Cr(III)aq-manganite (ɣ-MnOOH) interface: Simultaneous adsorption, microprecipitation, oxidation/reduction, and dissolution. Geochimica et Cosmochimica Acta. 2002;**66**:4119-4132

[72] Junta JL, Hochella Jr MF. Manganese(II) oxidation at mineral surfaces: A microscopic and spectroscopic study. Geochimica et Cosmochimica Acta. 1994;**58**:4985-4999

[73] Ha J, Trainor TP, Farges, F, Brown GE. Interaction of Zn (II) with hematite nanoparticles and microparticles: Part 2. ATR-FTIR and EXAFS study of the aqueous Zn(II)/oxalate/hematite ternary system. Langmuir. 2009;**25**:5586-5593

IntechOpen